

Precursor Tailoring Enables Alkylammonium Tin Halide Perovskite Phosphors for Solid-State Lighting

Ziliang Li, Zhengtao Deng,* Andrew Johnston, Jingwei Luo, Haijie Chen, Yitong Dong, Randy Sabatini, and Edward H. Sargent*

Broadband emission with a large Stokes shift is of interest for applications in solid-state lighting. Such emission is often achieved with self-trapped excitons; however, in reduced-dimensional perovskites, high-performance self-trapped emission has, until now, been widely observed only in lead-based materials. Here, the synthesis in an air ambient of reduced-dimensional Sn-based perovskite phosphors $R_{2+x}Sn_{1-x}I_{4+x}$ [R = octylammonium (OTA), hexylammonium (HA) or butylammonium (BA)] is reported, an advance achieved by tailoring the synthesis of the Ruddlesden-Popper 2D perovskites R_2SnI_4 . The lead-free $R_{2+x}Sn_{1-x}I_{4+x}$ phosphors have broadband self-trapped emission with over 80% photoluminescence quantum yield (PLQY) and more than a 150 nm Stokes shift. White-light-emitting diodes (WLEDs) based on $OTA_{2+x}Sn_{1-x}I_{4+x}$ phosphors exhibit warm-white emission (correlated color temperature = 2654K) suited to home lighting, and a CRI of 92, among the best for Pb-free perovskite WLEDs reported to date.

1. Introduction

Hybrid organic-inorganic halide perovskites have emerged as candidates for optoelectronic devices including solar cells,^[1–4] light-emitting diodes,^[5–8] and photodetectors^[9–11] due to their excellent optical and electrical properties, low-cost fabrication, and spectral tunability. By introducing bulky cations such as butylammonium (BA) and phenethylammonium (PEA), one may divide the 3D octahedra framework into corner-sharing octahedral layers, decreasing the dimensionality to two dimensions (2D). Slicing the 3D perovskite along the (001) plane results in Ruddlesden-Popper (RP) phases ($R_2A_{n-1}M_nX_{3n+1}$, R = 1+ cation)^[12–16] or Dion-Jacobson phases ($RA_{n-1}M_nX_{3n+1}$, R = 2+ cation)^[17–20] with flat (001) octahedral

sheets. The majority of 2D perovskites are either in the RP or the DJ phase; however, it is also possible to form perovskites by slicing the (110) plane of the 3D lattice.^[21–30] These perovskites are called corrugated 2D perovskites in light of the corrugated feature of the $[MX_6]^{4-}$ octahedral sheets. The dimensionality of the perovskite can be further reduced to one dimension (1D) where the octahedra form 1D chains^[24,25,31] and 0D^[32,33] where the octahedra are isolated by A cations.

Photoluminescence (PL) in 3D and 2D RP and DJ perovskites is based on band-edge recombination, and as a result exhibits a narrow full width at half maximum (FWHM) and a low Stokes shift;^[5–8,12,14] in contrast, broadband emission with a large Stokes shift is seen in 2D corrugated perovskites, 1D perovskites, and 0D perovskites.

The corrugated 2D lead halide perovskite (*N*-MEDA)PbBr₄ (*N*-MEDA = *N*¹-methylethane-1,2-diammonium) has been reported to have PL emission centered at 558 nm with a FWHM of 165 nm and a Stokes shift of 170 nm.^[21] (EDBE)PbBr₄ (EDBE = 2,2'-(ethylenedioxy)bis(ethylammonium)) evidenced a 9% PLQY with a FWHM of 215 nm.^[23] In addition, there have been reports of broadband emissive 1D C₄N₂H₁₄PbBr₄^[31] and 0D (C₄N₂H₁₄)₄SnBr₆ perovskites.^[34] Broadband emissive double halide perovskites Cs₂AgInCl₆ have also been reported, where Na and Bi doping breaks the dark transition and increases the PLQY.^[49]

Broadband emission originates from self-trapped excitons formed as a result of exciton-phonon coupling due to transient distortions of the lattice upon photoexcitation.^[35,36] Self-trapped emission is facilitated^[37] in lower-dimensional structures since these possess more vibrational degrees of freedom and are more easily polarized under photoexcitation.

Among low-dimensional perovskite and perovskite-like phosphors with broadband self-trapped emission, tin-based phosphors are of particular interest. Several broadband emissive tin-based phosphors with high PLQY (>80%) have been reported,^[32,34,38–40] and these have been found to be significantly brighter than the tin perovskites that rely on bandedge emission (PLQY ≤ 23%).^[41]

Unfortunately, Sn-based phosphors have, until now, relied on synthesis carried out in an inert atmosphere. As a result, the synthesis of Sn-based phosphors remains underexplored compared to their Pb-counterparts. In view of the large structural variability in low-dimensional hybrid halide perovskites, the

Z. Li, Z. Deng, A. Johnston, H. Chen, Y. Dong,^[†] R. Sabatini, E. H. Sargent
Department of Electrical and Computer Engineering
University of Toronto

10 King's College Road, Toronto, Ontario M5S 3G4, Canada
E-mail: dengz@njcu.edu.cn; ted.sargent@utoronto.ca

Z. Deng, J. Luo
College of Engineering and Applied Science
Nanjing National Laboratory of Microstructures
Nanjing University
Nanjing, Jiangsu 210093, P. R. China

 The ORCID identification number(s) for the author(s) of this article can be found under <https://doi.org/10.1002/adfm.202111346>.

^[†]Present address: Department of Chemistry and Biochemistry, University of Oklahoma, 101 Stephenson Parkway, Norman, OK 73019, USA

DOI: 10.1002/adfm.202111346

limited synthetic space indicates that there remains a large number of Sn-based compounds that are still to be investigated.

As one example, simply replacing the halide precursor leads to materials with completely different structures: (EDBE)PbCl₄ with RP 2D structure emerges when using Cl, compared to (EDBE)PbBr₄ with corrugated 2D structure when using Br.^[23] Multiple structures are obtainable with different synthetic conditions using the same precursors,^[25] or even from a single synthesis upon aging of the product.^[30]

We took the view that a facile synthesis process would allow judicious control over synthetic conditions, enabling us to tailor the structure and properties of new Sn-based materials.

Levering previously-reported air ambient synthesis of Sn-perovskites, we synthesized a series of new alkylammonium lead-free halide phosphors R_{2+x}SnI_{4+x} [R = octylammonium (OTA), hexylammonium (HA), or butylammonium (BA)]. We translated the synthesis of a previously-reported 2D RP perovskite (OTA)₂SnI₄^[39] into a new synthetic regime: we introduce excess alkylammonium ligand (OTA, HA, or BA) into the precursor solution with the goal of increasing the distortion of the lattice by increasing ligand incorporation. We pursued increased distortion toward the goal of increased self-trapped emission.^[35] We engineered the alkylammonium ligands with the goal of discovering additional Sn-based phases.

We find that the new R_{2+x}SnI_{4+x} compounds exhibit broadband emission with >80% PLQY, enabling their application in solid-state lighting; whereas the unmodified 2D RP perovskite R₂SnI₄ exhibits weak bandedge emission (PLQY < 1%). We also found an additional phase (BA₆SnI₈) when using BA as the excess ligand, one that exhibits weak broadband emission (PLQY < 1%).

2. Results and Discussion

Starting from a previously-reported synthetic method of (OTA)₂SnI₄,^[39] we dissolved precursors in an aqueous acid solution, which we then heated in the open air and cooled to achieve reprecipitation. Prior syntheses of tin-based perovskites have required inert gas environments to prevent oxidation; however, in the present approach, the use of an excess of hypophosphorous acid (HPA) enables ambient synthesis. HPA provides reducing conditions and inhibits oxidation of Sn²⁺ to Sn⁴⁺.^[44,50] A large quantity of dark-red crystals precipitated quickly upon cooling, and this led to weak red emission when samples were excited using a 375 nm UV lamp. However, after we aged the precipitate within the solution for over 1 h, we witnessed a new colorless phase with bright orange-yellow emission that appeared among the original dark-red crystals.

This result indicated that the original synthetic method of (OTA)₂SnI₄ yields two different phases with different crystallization rates. We posited that the bright orange-yellow emission may arise due to self-trapped excitons, as has been reported previously^[32,34,38–40] to result from a distorted lattice. To test this, we intentionally added additional OTA to the precursor solution, with the goal of increasing the lattice distortion and promoting the self-trapped emission phase. We found that the addition of OTA triggers the transition of the dark-red crystals to the colorless ones. We also found that this reaction was reversed when we added a small volume of water into the mixture. From this, we conclude that the two phases have different compositions,

and that the final product is tuned by tailoring the precursor ratio and solvent concentration.

We then synthesized both the pure colorless and dark-red compounds, which are the new 2D hybrid tin halide (OTA)_{2+x}SnI_{4+x} and Ruddlesden-Popper 2D perovskite (OTA)₂SnI₄, respectively. We denote the compounds OTA bright phase [(OTA)_{2+x}SnI_{4+x}] and OTA dark phase [(OTA)₂SnI₄] in light of their photoluminescence characteristics (Figure 1a and S1, Supporting Information). As self-trapped emission is more common in reduced-dimensional perovskites where the [MX₆] octahedra have a higher degree of distortion, we introduced excess octylamine to tune the dimensionality of the octahedra. The precursor octylamine/Sn ratio is increased from 4:1 to 30:1 in the synthesis of the bright phase; evaporation of the solvent (water) is significantly suppressed in the synthesis of the dark phase. In the absence of control over precursor ratio and the solvent concentration during reaction, the final product is a mixture of the two phases. We also replace tin(II) oxide with tin(II) halide (e.g., SnF₂) as the precursor tin source, as we find that tin(II) halides have higher solubility, and that product phase segregation is less likely when using tin(II) halides.

The precursor tailoring scheme is also applicable when the ligand is replaced with other bulky alkylammonium cations, including hexylammonium (HA) and butylammonium (BA). Synthesis using high hexylamine/Sn ratio (30:1) yields the HA bright phase [(HA)_{2+x}SnI_{4+x}], while low hexylamine/Sn ratio (4:1) with suppressed solvent evaporation yields the HA dark phase [(HA)₂SnI₄]. Regarding the BA-based synthesis, while low butylamine/Sn ratio still leads to the formation of the BA dark phase [(BA)₂SnI₄], increasing the butylamine/Sn ratio will lead to the formation of a phase with weak orange-red emission (Figure 1b). The chemical formula of this phase is BA₆SnI₈, as determined using single-crystal X-ray diffraction (SCXRD). HA₆SnI₈ and OTA₆SnI₈, other than the bright phases (R_{2+x}SnI_{4+x}) and the dark phases (R₂SnI₄), were not obtained at any alkylamine/Sn ratio used in the synthesis. The BA bright phase [(BA)_{2+x}SnI_{4+x}], which has similar structural and photophysical properties to the OTA and HA bright phases, was synthesized by aging, for 48 h, the wet BA₆SnI₈ precipitate obtained after we discarded the supernatant.

The crystalline structure of the resultant compounds was characterized using powder X-ray diffraction (PXRD, Figure 2a–c). All compounds except BA₆SnI₈ show periodic diffraction peaks, denoted (00k) reflections in layered 2D structures. Table 1 summarizes the layer-to-layer spacing of each compound calculated according to Bragg's law. Both the bright and the dark phases experienced a reduction in the layer-to-layer spacing when the alkylammonium cation was switched to a shorter one. For phases with the same alkylammonium cation, the bright phase always has larger layer spacing compared to the dark phase; however, the <10% difference of the spacing indicates the structural similarity between each of the bright and the dark phases.

The layered morphology was observed for both dark and bright phases under the optical microscope (Figure S3–S6, Supporting Information) and scanning electron microscope (SEM, Figure S7, Supporting Information). While the OTA bright phase features high crystallinity with hexagonal layers, the HA bright phase, and the BA bright phase feature rectangular layers. As was reported previously, the crystal structure of tin-based RP 2D perovskites is similar to their lead-based counterparts. There is only a 0.03% difference in the metal halide

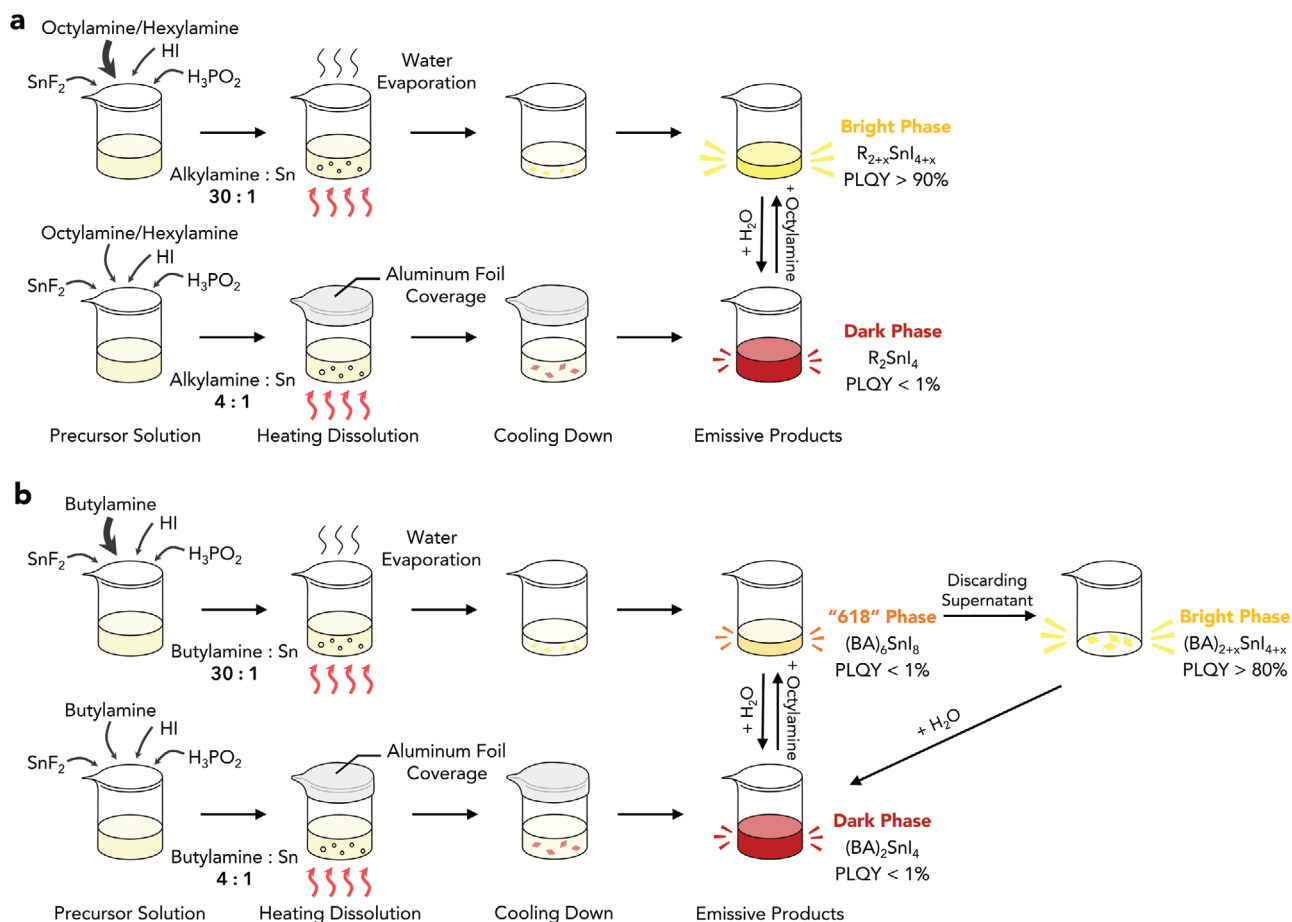


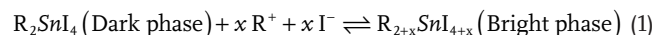
Figure 1. Precursor tailoring enables the synthesis and separation of a) OTA- or HA-based compounds $R_{2+x}SnI_{4+x}$ (bright phase) and R_2SnI_4 (dark phase), and b) BA-based compounds $BA_{2+x}SnI_{4+x}$ (BA bright phase), BA_2SnI_4 (BA dark phase), and BA_6SnI_8 .

octahedra layer spacing (d_{002} spacing), between $(BA)_2SnI_4$ (BA = butylammonium) and $(BA)_2PbI_4$.^[16] According to a recent study of Ruddlesden-Popper phase lead halide perovskites, the d_{002} spacing of the room-temperature $(OTA)_2PbI_4$ phase is 18.7 Å.^[15] We conclude that the dark phase with a d_{002} spacing of 18.8 Å is the RP 2D perovskite $(OTA)_2SnI_4$. The 18.8 Å layer spacing consists of a monolayer of corner-sharing $[SnI_6]$ octahedra which is ≈ 6.4 Å, and two intercalating octylammonium cation layers of length 12.4 Å (Figure S2, Supporting Information). Likewise, the HA dark phase with a d_{002} spacing of 16.3 Å and the BA dark phase with a d_{002} spacing of 13.7 Å represent the RP 2D perovskite $(HA)_2SnI_4$ and $(BA)_2SnI_4$, respectively.

The single-crystal structure of the BA_6SnI_8 phase was determined using SCXRD, and the corresponding bond distance and angles are listed in Table S1–S2, Supporting Information. In contrast with the 2D dark and bright phases, the BA_6SnI_8 phase is a compound with a 0D perovskite structure, where the $[SnI_6]$ octahedra are isolated and surrounded by BA cations and iodide ions (Figure 2d).^[42] This structure is similar to previously-reported 0D Sn-based perovskites.^[32,33,38]

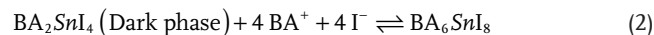
Using Energy-dispersive X-ray spectroscopy (EDS) we investigated the elemental composition of the OTA-based compounds. As shown in Figures S8 and S9, Supporting Information, the bright phase has a higher I:Sn ratio compared to the dark phase. As EDS provides semi-quantitative analysis for elemental composition, we

were not able to determine the stoichiometry of the OTA bright phase accurately. As a result, we refer to the chemical formula of the OTA bright phase as $(OTA)_{2+x}SnI_{4+x}$, where x is a positive value. Considering structural similarities, the chemical formula of the HA and BA bright phases is proposed to be $(HA)_{2+x}SnI_{4+x}$ and $(BA)_{2+x}SnI_{4+x}$. Therefore, the transitions between the bright and dark phases ($R = OTA$ or HA) are expressed as:



When we add an appropriate amount of octylamine/hexylamine to the vial containing the OTA/HA dark phase, the protonated OTA/HA cation shifts the equilibrium to the right, promoting the formation of the bright phase. When we dissolve the bright phase using water, we find that OTA/HA has a strong tendency to dissociate from the $R_{2+x}SnI_{4+x}$ lattice and be solvated by water molecules, promoting the transition from the bright phase to the dark phase.

When using BA as the alkylammonium ligand, similar transitions between the dark phase and the bright phase or BA_6SnI_8 phase are seen:



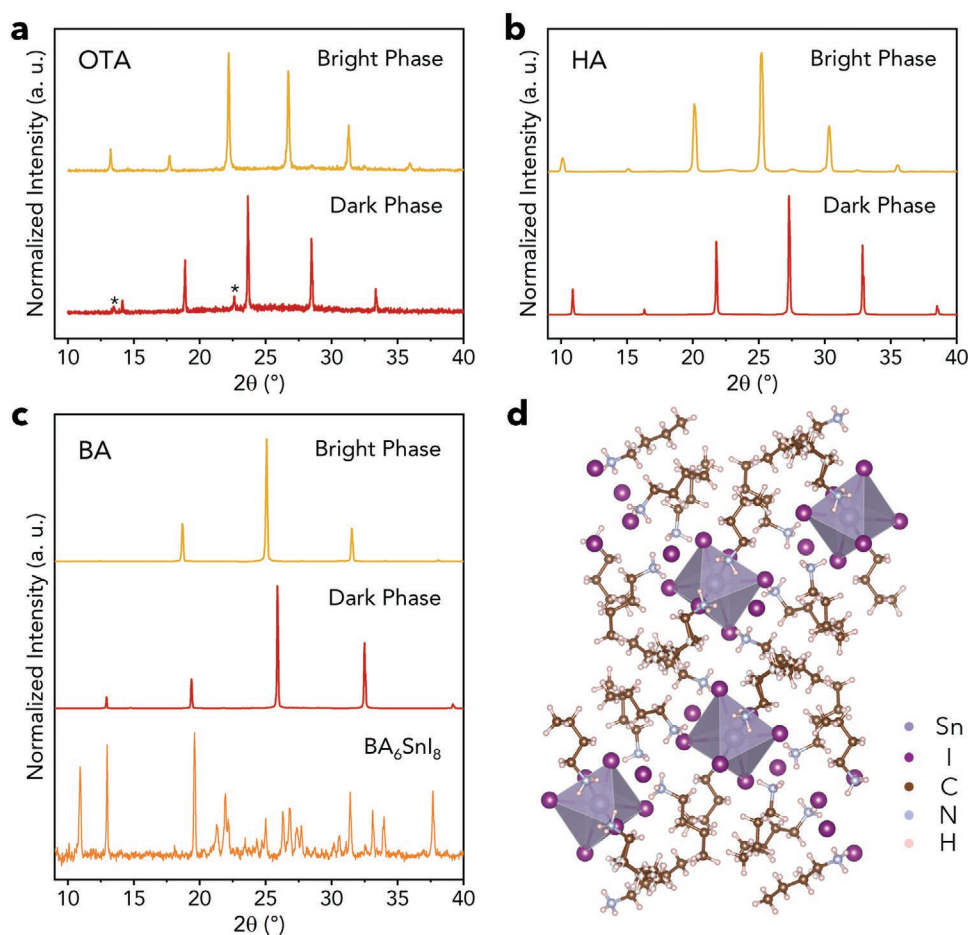


Figure 2. Powder XRD pattern of a) OTA-based, b) HA-based and c) BA-based compounds. Asterisks (*) indicate peaks of residual (OTA)I precursor in the $(\text{OTA})_2\text{SnI}_4$ sample. d) Single-crystal structure of 0D perovskite BA_6SnI_8 viewing from the a-axis, visualized through VESTA.^[42]

BA_6SnI_8 can be synthesized by adding an appropriate amount of butylamine to the BA dark phase and can be transformed back to the BA dark phase by dissolving with water. As discussed previously, BA bright phase could not be synthesized by transition from BA dark phase directly; however, it can be easily transformed to the dark phase through addition of water, which is analogous to the OTA and HA bright phases.

We also investigated the Sn oxidation state for the OTA bright phase and the dark phase using X-ray photoelectron spectroscopy (XPS) (Figure S10, Supporting Information). XPS probes to a depth of ≈ 10 nm and provides as a result compositional information within this distance from the surface of the samples. We fit two peaks at 494.5 and 486.1 eV, which were identified as the spin-orbit splitting of electrons from the $3d_{3/2}$ and $3d_{5/2}$ states of Sn^{2+} , respectively (Figure S10a, Supporting Information). The additional two peaks at 496.8 and 488.2 eV in the dark phase sample were identified as the Sn 3d doublets corresponding to Sn^{4+} states,^[43,44] a finding we attribute to partial oxidation of the surface of the sample (Figure S10b, Supporting Information). These Sn^{4+} peaks were not found in the OTA bright phase sample, an indication that the bright phase was not oxidized upon synthesis. To compare further the stability of the bright and the dark phase, we acquired XPS for

OTA bright phase and dark phase samples that have been stored in ambient air for 24 h. The Sn^{2+} at the surface of the dark phase had fully oxidized to Sn^{4+} (Figure S10d, Supporting Information), while Sn^{2+} at the surface of the bright phase was only partially oxidized (Figure S10c, Supporting Information). It is expected that the surface of the samples has a higher Sn^{4+} percentage compared to the interior, as the oxidation process starts from the surface of the crystals. Although Sn^{2+} of both the OTA bright phase and dark phase will be partially oxidized to Sn^{4+} after exposure in air, this process is significantly suppressed in the bright phase. We hypothesize that the increased percentage of OTA ligand surrounding the $[\text{SnI}_6]$ octahedra in the bright phase retards the oxidation of Sn^{2+} more efficiently, thus improving its stability in ambient air. In contrast, in the

Table 1. Layer-to-layer spacing of the 2D alkylammonium based compounds (Unit: Å).

Alkylammonium type	Bright phase	Dark phase
OTA-based	20.0	18.8
HA-based	17.6	16.3
BA-based	14.2	13.7

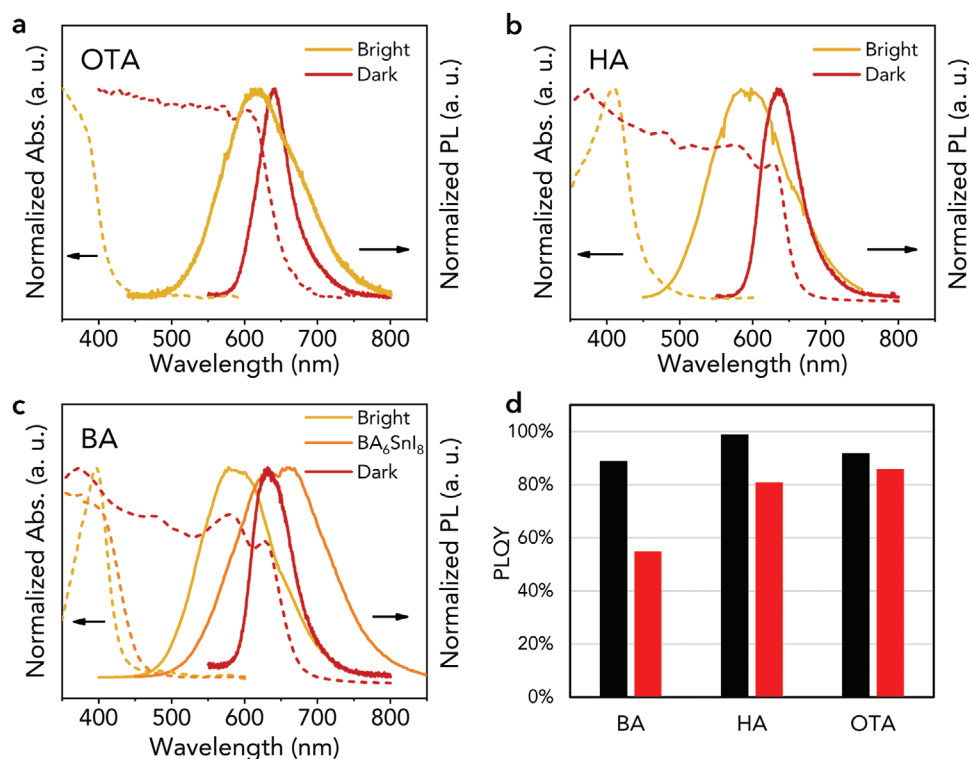


Figure 3. UV-vis absorption spectra (dashed line) and PL spectra (solid line) of a) OTA-based, b) HA-based and c) BA-based compounds. d) PLQY of OTA, HA, and BA bright phases measured upon synthesis (black) and after ambient storage for 15 days (red).

dark phase, Sn^{2+} oxidation introduces Sn vacancies that have the potential to act as nonradiative recombination centers and quench emission.^[44,51,52] As the percentage of alkylammonium ligand in the HA and BA bright phases is also higher than their dark phase counterparts, their stability in ambient air is also expected to be improved.

The optical properties of compounds were characterized using UV-vis absorption and photoluminescence (PL) spectra (Figure 3a–c and Table 2). The dark phases have narrow PL peaks centered at 632–640 nm with small Stokes shifts, showing bandedge recombination typical of RP 2D perovskites. Unlike the dark phases, the bright phases absorb primarily UV and deep-blue light. Plots of $(\alpha h\nu)^2$ versus photon energy indicate significant bandgap differences between the bright phases and the dark phases (Figure S11, Supporting Information). The broad PL peaks of the bright phases are centered at 578–617 nm with FWHM of over 120 nm and Stokes shifts of

Table 2. Summary of photoluminescence properties.

Alkylammonium type	Phase	PL peak [nm]	FWHM [nm]	PLQY [%]
OTA	Bright phase	617	128	92
	Dark phase	640	51	<1
HA	Bright phase	598	126	99
	Dark phase	633	59	<1
BA	Bright phase	578	120	89
	Dark phase	632	61	<1
	BA_6SnI_8	662	150	<1

over 150 nm. The bright phases exhibit high PLQYs of over 80%, among which the HA bright phase reaches the highest PLQY of 99%. To investigate the stability of bright phases with different alkylammonium cations, we also measured PLQY after storing the samples in ambient air ($\approx 30\%$ relative humidity) for 15 days. The PLQY of BA and HA bright phase dropped to 55% and 81%, respectively. The PLQY of the OTA bright phase dropped by 6% (Figure 3d). The bright phases show enhanced stability when stored in ambient air together with the mother liquor containing HPA. After six months, the OTA bright phase exhibits a 5% relative decrease in PLQY, and a spectral shift less than 10 nm (Figure S12, Supporting Information). We hypothesize that the relative stability of the OTA bright phase can be attributed to the use of long alkylammonium chains in the crystals. Three-dimensional excitation-emission matrix (EEM) fluorescence spectroscopy further confirmed that there was no PL peak shift when varying the excitation wavelength (Figure S13, Supporting Information). This suggests that no extra energy level or other impurities existed in the bright phase samples.^[39] As in the case of the bright phases, the BA_6SnI_8 phase exhibits broadband emission and a large Stokes shifts (>200 nm), albeit with a redder PL peak (662 nm) and low PLQY beyond the detection limit ($<1\%$).

The broad PL peaks taken together with large Stokes shifts suggest that exciton self-trapping is the dominant emission mechanism for the bright phases and the BA_6SnI_8 phase. Time-resolved PL spectra of the bright phases measured at the PL peak wavelength can be fit to a single exponential decay function with a lifetime of 1.2 μs (Figure S14a,c,e, Supporting Information). The microsecond scale of lifetimes matches well with the timescale of

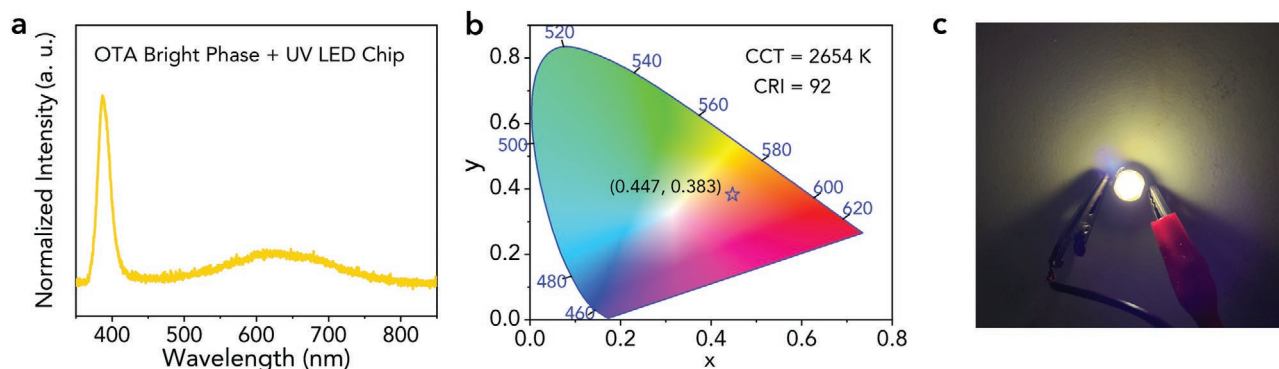


Figure 4. Tin halide perovskite phosphors for white LEDs. a) Luminescence spectra of UV LED-pumped OTA bright phase phosphor in the polystyrene (PS) matrix. b) Chromaticity coordinates of the white LEDs plotted on the CIE1931 chromaticity chart. c) Image of an UV LED-pumped tin halide perovskite white LED.

previously-reported lifetime values of phosphors with self-trapped emission.^[34,39] In contrast, the dark phases exhibit lifetimes on a nanosecond scale, which are characteristics of band-edge emission (Figure S14b,d,g, Supporting Information). The self-trapped emission mechanism of the bright phases was also confirmed by studying the dependence of PL on excitation intensity (Figure S15, Supporting Information). A femtosecond laser fixed at 375 nm emission was used as the excitation source, and the PL intensity of each bright phase increases linearly with excitation power density from 10 to 198 mW cm⁻² at room temperature. The absence of PL saturation indicates that the emission does not arise from permanent defects, but instead from self-trapped excitons that act as excited-state defects.^[23] Although the PL decay lifetime of the BA₆SnI₈ phase is sub-microsecond (Figure S14f, Supporting Information), the linear dependence of PL intensity on excitation power intensity accords with the self-trapped emission mechanism. For the OTA bright phase, femtosecond transient absorption (TA) spectra further confirmed the self-trapped mechanism. A broad pump-induced absorption, a typical TA feature for self-trapped excitons,^[45–47] is observed following 380 nm photoexcitation (Figure S16, Supporting Information). Each wavelength feature exhibits the same turn-on time (\approx 400 fs), one that we associate with the time to form self-trapped excitons.^[46]

The broadband emission and high PLQY enable application for these lead-free R₂+_xSnI₄+_x phosphors in solid-state lighting. We selected the OTA bright phase as the phosphor to prepare white light emitting diodes (LEDs). We incorporated the phosphor into a polystyrene (PS) matrix and

photoexcited the phosphor-PS composite using a 387 nm UV LED (Figure 4a). The LEDs have Commission Internationale de l'Éclairage (CIE) coordinates (0.447, 0.383) with correlated color temperature (CCT) of 2654 K, corresponding to warm-white light as desired in home lighting (Figure 4b). The devices also achieve a high color rendering index (CRI) of 92: this is among the best reported Pb-free perovskite white LEDs (Table 3). The large Stokes shift of the OTA bright phase minimizes energy loss due to reabsorption.^[48] The color temperature of the white LEDs is tunable by the addition of blue phosphors. White LEDs based on mixed OTA bright phase/BaMgAl₁₀O₁₇:Eu²⁺ phosphors exhibit a cooler color temperature of \approx 3300 K (Figure S17, Supporting Information). To test the operating stability of these white LEDs, we tracked the luminescence spectra of the devices under continuous UV light excitation. The white LEDs exhibit no significant luminescence decay (<2% relative) over 25 min (Figure S18, Supporting Information).

3. Conclusions

We report the synthesis of a series of new 2D alkylammonium tin(II) halide perovskites R₂+_xSnI₄+_x [R = octylammonium (OTA), hexylammonium (HA), or butylammonium (BA)] which exhibit broad self-trapped emission with PLQY of more than 80% and Stokes shifts of more than 150 nm. The facile and scalable synthesis procedure, combined with good optical properties, enables the application of these materials in solid-state lighting.

Table 3. Summary of the representative Pb-free perovskite white LEDs.

Phosphors	CIE coordinates	CCT [K]	CRI	Reference
(C ₄ N ₂ H ₁₄ Br) ₄ SnBr ₃ I ₃ + Ba _{0.86} Eu _{0.14} MgAl ₁₀ O ₁₇	(0.32, 0.32)	6160	84	[32]
(C ₄ N ₂ H ₁₄ Br) ₄ SnBr ₆ + BaMgAl ₁₀ O ₁₇ :Eu ²⁺	(0.35, 0.39)	4946	70	[34]
(C ₈ H ₂₀ N) ₂ SnBr ₄ + BaMgAl ₁₀ O ₁₇ :Eu ²⁺ + Eu doped silicates	(0.33, 0.31)	6530	89	[39]
(C ₆ H ₁₈ N) ₃ SnBr ₈ + BaMgAl ₁₀ O ₁₇ :Eu ²⁺ , Mn ²⁺	(0.36, 0.30)	5700	94	[40]
Cs ₂ Ag _{0.6} Na _{0.4} InCl ₆ :Bi ³⁺	(0.40, 0.45)	4054	-	[49]
(OTA) _{2+x} SnI _{4+x}	(0.45, 0.38)	2654	92	This work

4. Experimental Section

Materials: Tin(II) oxide (Sigma-Aldrich, 99.99%), Tin(II) fluoride (Sigma-Aldrich, 99%), *n*-octylamine (Sigma-Aldrich, 99%), *n*-hexylamine (Sigma-Aldrich, 99%), *n*-butylamine (Sigma-Aldrich, 99.5%), hydroiodic acid (HI, Sigma-Aldrich, 57 wt. % in H₂O), hypophosphorous acid (HPA, Sigma-Aldrich, 50 wt. % in H₂O) and BaMgA₁₀O₁₇:Eu²⁺ phosphor (Shenzhen Looking Long Technology Co., Ltd.) were purchased and used as procured without further purification.

Synthesis of (OTA)_{2+x}SnI_{4+x}, (HA)_{2+x}SnI_{4+x} and (BA)₆SnI₈: 0.375 mmol SnF₂ powder was dissolved in 1.25 ml HI by sonication until all SnF₂ powder was dissolved. Then 3.75 ml HPA was added to prevent the oxidation of the tin(II), with further sonication of 30 min. After sonification, 11.25 mmol *n*-octylamine was added to the SnF₂ + HI + HPA stock solution under strong agitation in a 100 ml beaker. The solution was heated to 100 °C and maintained for 15 min without covering the beaker. Finally, the solution was slowly cooled down to room temperature in 24 h and the colorless plate-like OTA bright phase crystals were formed gradually. Synthesis of (HA)_{2+x}SnI_{4+x} and (BA)₆SnI₈ follow the same steps, except that the addition of *n*-octylamine was replaced with equimolar *n*-hexylamine and *n*-butylamine, respectively.

Synthesis of (BA)_{2+x}SnI_{4+x}: After getting the BA₆SnI₈ precipitate from the precursor solution, the supernatant was discarded, and the remaining precipitate was aged for 24–48 h until all the precipitate was transformed to the BA bright phase.

Synthesis of (OTA)₂SnI₄, (HA)₂SnI₄ and (BA)₂SnI₄: 0.375 mmol SnF₂ powder was dissolved in 1.25 ml HI by sonication until all SnF₂ powder was dissolved. Then 3.75 ml HPA was added to prevent the oxidation of the tin(II), with further sonication of 30 min. After sonification, 1.5 mmol *n*-octylamine was added to the SnF₂ + HI + HPA stock solution under strong agitation in a 100 ml beaker. Then the solution was heated to 100 °C and maintained for 15 min with aluminum foil covering the beaker to retain the evaporating water. Finally, the solution was cooled down at 0 °C ice bath and the dark-red plate-like (OTA)₂SnI₄ crystals were formed gradually. Synthesis of (HA)₂SnI₄ and (BA)₂SnI₄ followed the same steps except that addition of *n*-octylamine was replaced with equimolar *n*-hexylamine and *n*-butylamine, respectively.

White LED Fabrication: OTA_{2+x}SnI_{4+x} phosphors were blended with 25% PS dissolved in dichloromethane. The blended phosphor-PS paste was deposited on 387 nm UV LED chips (1 W) and dried in air to form white LEDs. For white LEDs with a cooler color temperature (≈3300 K), the phosphors contain a mixture of OTA_{2+x}SnI_{4+x} and BaMgA₁₀O₁₇:Eu²⁺. The blended phosphor-PS paste was deposited on 375 nm UV LED chips.

Absorption Measurements: Optical absorption spectra were measured with a Perkin Elmer 950 UV-Vis-NIR spectrometer equipped with an integrating sphere for thin-film measurements.

Fluorescence Microscopy: Fluorescence microscope images were captured through Axio Vert A1 FL-LED at room temperature.

Scanning Electron Microscopy and Energy Dispersive X-Ray Spectroscopy: SEM and EDS were performed on a JEOL JSM-7800F at 10 kV.

Powder X-Ray Diffraction Measurements: Powder X-ray diffractograms were recorded using a Rigaku MiniFlex 600 powder X-ray diffractometer equipped with a NaI scintillation counter and using monochromatized Cu K α radiation ($\lambda = 1.5406 \text{ \AA}$), with a detector angle (2θ) step of 0.02°.

Single-Crystal X-Ray Diffraction Measurements: Single crystal X-ray diffraction data of BA₆SnI₈ crystal were collected at 100 K on a Bruker Kappa APEX-DUO diffractometer equipped with a rotating anode with graphite-monochromated Mo-K α radiation (Burker Triumph, $\lambda = 0.71073 \text{ \AA}$), as well as a low-temperature Oxford Cryosystem apparatus.

X-Ray Photoelectron Spectroscopy Measurements: X-ray photoelectron spectroscopy measurements were carried out on a ThermoFisher Scientific K-Alpha spectrometer, using Al K α X-ray radiation (1486.6 eV) for excitation.

Transient Absorption Measurements: Femtosecond laser pulses of a 380 nm fundamental beam at a 5 kHz repetition rate were produced using a regenerative amplified Yb:KGW laser (PHAROS, Light Conversion). Part of the fundamental beam was used to pump an optical parametric

amplifier (ORPHEUS, Light Conversion) to serve as a narrowband pump, while the other part was focused on a sapphire crystal to generate a white-light supercontinuum probe (400–1000 nm window with various optical filters). Both the pump and probe pulses were directed into a commercial TA spectrometer (Helios, Ultrafast). Delaying the probe pulse relative to the pump provides a time window of up to 2.5 ps.

Photoluminescence Measurements: PL spectra were recorded using a Horiba Fluorolog system equipped with a single grating and a time-correlated single photon counting detector. For steady-state PL measurements, the excitation source is a monochromated Xe lamp. For time-resolved PL, a 374 nm laser diode was used with the overall time resolution of $\Delta t \approx 1.756 \text{ ns}$ (for OTA, HA, and BA bright phases) and $\Delta t \approx 0.220 \text{ ns}$ (for BA₆SnI₈).

PLQY Measurements: PLQY measurements were done by coupling a Quanta-Phi integrating sphere to the Horiba Fluorolog system with optical fiber bundles. A monochromated Xe lamp is used as the excitation source. Both excitation and emission spectra were collected for the two cases of the sample directly illuminated by the excitation beam path in the integrating sphere and the empty sphere itself. The Fluorolog was set to an excitation wavelength of 380 nm and to have a 5 nm bandpass for both the excitation and emission slits. The detector and integrating sphere were corrected for spectral variance using a calibrated white light source. The PLQY was calibrated using standard materials with known PLQY values and emission covering the measurement range, including Coumarin 6, Coumarin 153, and Rhodamine 6G.

Excitation-Emission Matrix Fluorescence Spectroscopy: EEM was obtained from a Hamamatsu Photonics Quantaurus-QY (model: C11347-11) under ambient conditions.

Excitation Intensity Dependent PL Measurements: PL spectra were recorded using Ocean Optics USB 2000. The excitation source was femtosecond laser pulses of a 375 nm fundamental beam at a 5 kHz repetition rate, which were produced using a regenerative amplified Yb:KGW laser (PHAROS, Light Conversion).

[CCDC 2053856 contains the supplementary crystallographic data for this paper. These data can be obtained free of charge from The Cambridge Crystallographic Data Centre via www.ccdc.cam.ac.uk/data_request/cif]

Supporting Information

Supporting Information is available from the Wiley Online Library or from the author.

Acknowledgements

Z.L. and Z.D. contributed equally to this work. This publication was based in part on work supported by the Ontario-Jiangsu Industrial R&D Program (OJIRDP). E.H.S. and all co-authors from the Department of Electrical and Computer Engineering at the University of Toronto acknowledge the financial support from the Ontario Research Fund-Research Excellence Program. Z.D. acknowledge the financial support from the Natural Science Foundation of China (22075129). The authors acknowledge the technical assistance and scientific guidance of Dr. Alan Lough, Dr. Golam Bappi, and Yuan Liu at the University of Toronto.

Conflict of Interest

The authors declare no conflict of interest.

Data Availability Statement

The data that support the findings of this study are available from the corresponding author upon reasonable request.

Keywords

lead-free, low-dimensional structures, perovskites, self-trapped excitons, solid-state lighting

Received: November 22, 2021

Revised: December 30, 2021

Published online:

- [1] H. Zhou, Q. Chen, G. Li, S. Luo, T.-b. Song, H.-S. Duan, Z. Hong, J. You, Y. Liu, Y. Yang, *Science* **2014**, 345, 542.
- [2] A. Kojima, K. Teshima, Y. Shirai, T. Miyasaka, *J. Am. Chem. Soc.* **2009**, 131, 6050.
- [3] M. Liu, M. B. Johnston, H. J. Snaith, *Nature* **2013**, 501, 395.
- [4] H. Tan, A. Jain, O. Voznyy, X. Lan, F. P. G. De Arquer, J. Z. Fan, R. Quintero-Bermudez, M. Yuan, B. Zhang, Y. Zhao, *Science* **2017**, 355, 722.
- [5] M. Yuan, L. N. Quan, R. Comin, G. Walters, R. Sabatini, O. Voznyy, S. Hoogland, Y. Zhao, E. M. Beaugard, P. Kanjanaboos, Z. Lu, D. H. Kim, E. H. Sargent, *Nat. Nanotechnol.* **2016**, 11, 872.
- [6] N. Wang, L. Cheng, R. Ge, S. Zhang, Y. Miao, W. Zou, C. Yi, Y. Sun, Y. Cao, R. Yang, Y. Wei, Q. Guo, Y. Ke, M. Yu, Y. Jin, Y. Liu, Q. Ding, D. Di, L. Yang, G. Xing, H. Tian, C. Jin, F. Gao, R. H. Friend, J. Wang, W. Huang, *Nat. Photonics* **2016**, 10, 699.
- [7] S. D. Stranks, H. J. Snaith, *Nat. Nanotechnol.* **2015**, 10, 391.
- [8] Z. Xiao, R. A. Kerner, L. Zhao, N. L. Tran, K. M. Lee, T.-W. Koh, G. D. Scholes, B. P. Rand, *Nat. Photonics* **2017**, 11, 108.
- [9] L. Dou, Y. M. Yang, J. You, Z. Hong, W.-H. Chang, G. Li, Y. Yang, *Nat. Commun.* **2014**, 5, 5404.
- [10] M. I. Saidaminov, V. Adinolfi, R. Comin, A. L. Abdelhady, W. Peng, I. Dursun, M. Yuan, S. Hoogland, E. H. Sargent, O. M. Bakr, *Nat. Commun.* **2015**, 6, 7586.
- [11] Y. Fang, Q. Dong, Y. Shao, Y. Yuan, J. Huang, *Nat. Photonics* **2015**, 9, 679.
- [12] C. C. Stoumpos, D. H. Cao, D. J. Clark, J. Young, J. M. Rondinelli, J. I. Jang, J. T. Hupp, M. G. Kanatzidis, *Chem. Mater.* **2016**, 28, 2852.
- [13] D. H. Cao, C. C. Stoumpos, T. Yokoyama, J. L. Logsdon, T.-B. Song, O. K. Farha, M. R. Wasielewski, J. T. Hupp, M. G. Kanatzidis, *ACS Energy Lett.* **2017**, 2, 982.
- [14] D. H. Cao, C. C. Stoumpos, O. K. Farha, J. T. Hupp, M. G. Kanatzidis, *J. Am. Chem. Soc.* **2015**, 137, 7843.
- [15] A. Lemmerer, D. G. Billing, *Dalton Trans.* **2012**, 41, 1146.
- [16] D. B. Mitzi, *Chem. Mater.* **1996**, 8, 791.
- [17] L. Mao, W. Ke, L. Pedesseau, Y. Wu, C. Katan, J. Even, M. R. Wasielewski, C. C. Stoumpos, M. G. Kanatzidis, *J. Am. Chem. Soc.* **2018**, 140, 3775.
- [18] P. Li, X. Liu, Y. Zhang, C. Liang, G. Chen, F. Li, M. Su, G. Xing, X. Tao, Y. Song, *Angew. Chem., Int. Ed. Engl.* **2020**, 59, 6909.
- [19] M. Chen, M.-G. Ju, M. Hu, Z. Dai, Y. Hu, Y. Rong, H. Han, X. C. Zeng, Y. Zhou, N. P. Padture, *ACS Energy Lett.* **2018**, 4, 276.
- [20] S. Ahmad, P. Fu, S. Yu, Q. Yang, X. Liu, X. Wang, X. Wang, X. Guo, C. Li, *Joule* **2019**, 3, 794.
- [21] E. R. Dohner, E. T. Hoke, H. I. Karunadasa, *J. Am. Chem. Soc.* **2014**, 136, 1718.
- [22] D. Mitzi, S. Wang, C. Feild, C. Chess, A. Guloy, *Science* **1995**, 267, 1473.
- [23] E. R. Dohner, A. Jaffe, L. R. Bradshaw, H. I. Karunadasa, *J. Am. Chem. Soc.* **2014**, 136, 13154.
- [24] L. Mao, P. Guo, M. Kepenekian, I. Hadar, C. Katan, J. Even, R. D. Schaller, C. C. Stoumpos, M. G. Kanatzidis, *J. Am. Chem. Soc.* **2018**, 140, 13078.
- [25] C. C. Stoumpos, L. Mao, C. D. Malliakas, M. G. Kanatzidis, *Inorg. Chem.* **2017**, 56, 56.
- [26] M. Daub, C. Haber, H. Hillebrecht, *Eur. J. Inorg. Chem.* **2017**, 2017, 1120.
- [27] J. Guan, Z. Tang, A. M. Guloy, *Chem. Commun.* **1999**, 1833.
- [28] Y. Li, C. Lin, G. Zheng, Z. Cheng, H. You, W. Wang, J. Lin, *Chem. Mater.* **2006**, 18, 3463.
- [29] Y. Li, G. Zheng, J. Lin, *Eur. J. Inorg. Chem.* **2008**, 2008, 1689.
- [30] L. Mao, Y. Wu, C. C. Stoumpos, M. R. Wasielewski, M. G. Kanatzidis, *J. Am. Chem. Soc.* **2017**, 139, 5210.
- [31] C. Zhou, Y. Tian, M. Wang, A. Rose, T. Besara, N. K. Doyle, Z. Yuan, J. C. Wang, R. Clark, Y. Hu, T. Siegrist, S. Lin, B. Ma, *Angew. Chem., Int. Ed. Engl.* **2017**, 56, 9018.
- [32] C. Zhou, Y. Tian, Z. Yuan, H. Lin, B. Chen, R. Clark, T. Dilbeck, Y. Zhou, J. Hurley, J. Neu, T. Besara, T. Siegrist, P. Djurovich, B. Ma, *ACS Appl. Mater. Interfaces* **2017**, 9, 44579.
- [33] C. Zhou, H. Lin, H. Shi, Y. Tian, C. Pak, M. Shatruk, Y. Zhou, P. Djurovich, M. H. Du, B. Ma, *Angew. Chem., Int. Ed. Engl.* **2018**, 57, 1021.
- [34] C. Zhou, H. Lin, Y. Tian, Z. Yuan, R. Clark, B. Chen, L. J. van de Burgt, J. C. Wang, Y. Zhou, K. Hanson, Q. J. Meisner, J. Neu, T. Besara, T. Siegrist, E. Lambers, P. Djurovich, B. Ma, *Chem. Sci.* **2018**, 9, 586.
- [35] M. D. Smith, H. I. Karunadasa, *Acc. Chem. Res.* **2018**, 51, 619.
- [36] B. Saparov, D. B. Mitzi, *Chem. Rev.* **2016**, 116, 4558.
- [37] H. Lin, C. Zhou, Y. Tian, T. Siegrist, B. Ma, *ACS Energy Lett.* **2017**, 3, 54.
- [38] L.-J. Xu, H. Lin, S. Lee, C. Zhou, M. Worku, M. Chaaban, Q. He, A. Plaviak, X. Lin, B. Chen, M.-H. Du, B. Ma, *Chem. Mater.* **2020**, 32, 4692.
- [39] A. Wang, Y. Guo, Z. Zhou, X. Niu, Y. Wang, F. Muhammad, H. Li, T. Zhang, J. Wang, S. Nie, Z. Deng, *Chem. Sci.* **2019**, 10, 4573.
- [40] P. Fu, M. Huang, Y. Shang, N. Yu, H.-L. Zhou, Y.-B. Zhang, S. Chen, J. Gong, Z. Ning, *ACS Appl. Mater. Interfaces* **2018**, 10, 34363.
- [41] J.-T. Lin, Y.-K. Hu, C.-H. Hou, C. C. Liao, W.-T. Chuang, C.-W. Chiu, M.-K. Tsai, J.-J. Shyue, P.-T. Chou, *Small* **2021**, 16, 2000903.
- [42] K. Momma, F. Izumi, *J. Appl. Crystallogr.* **2011**, 44, 1272.
- [43] Y. Wang, R. Zou, J. Chang, Z. Fu, Y. Cao, L. Zhang, Y. Wei, D. Kong, W. Zou, K. Wen, *J. Phys. Chem. Lett.* **2019**, 10, 453.
- [44] H. Liang, F. Yuan, A. Johnston, C. Gao, H. Choubisa, Y. Gao, Y. K. Wang, L. K. Sagar, B. Sun, P. Li, *Adv. Sci.* **2020**, 7, 1903213.
- [45] L. Zhou, J. F. Liao, Z. G. Huang, J. H. Wei, X. D. Wang, H. Y. Chen, D. B. Kuang, *Angew. Chem., Int. Ed. Engl.* **2019**, 58, 15435.
- [46] T. Hu, M. D. Smith, E. R. Dohner, M. J. Sher, X. Wu, M. T. Trinh, A. Fisher, J. Corbett, X. Y. Zhu, H. I. Karunadasa, A. M. Lindenberg, *J. Phys. Chem. Lett.* **2016**, 7, 2258.
- [47] B. B. Cui, Y. Han, B. Huang, Y. Zhao, X. Wu, L. Liu, G. Cao, Q. Du, N. Liu, W. Zou, M. Sun, L. Wang, X. Liu, J. Wang, H. Zhou, Q. Chen, *Nat. Commun.* **2019**, 10, 5190.
- [48] S. Li, J. Luo, J. Liu, J. Tang, *J. Phys. Chem. Lett.* **2019**, 10, 1999.
- [49] J. Luo, X. Wang, S. Li, J. Liu, Y. Guo, G. Niu, L. Yao, Y. Fu, L. Gao, Q. Dong, C. Zhao, M. Leng, F. Ma, W. Liang, L. Wang, S. Jin, J. Han, L. Zhang, J. Etheridge, J. Wang, Y. Yan, E. H. Sargent, J. Tang, *Nature* **2018**, 563, 541.
- [50] W. Li, J. Li, J. Li, J. Fan, Y. Mai, L. Wang, *J. Mater. Chem. A* **2016**, 4, 17104.
- [51] Y. Wang, R. Zou, J. Chang, Z. Fu, Y. Cao, L. Zhang, Y. Wei, D. Kong, W. Zou, K. Wen, N. Fan, N. Wang, W. Huang, J. Wang, *J. Phys. Chem. Lett.* **2019**, 10, 453.
- [52] M. H. Kumar, S. Dharani, W. L. Leong, P. P. Boix, R. R. Prabhakar, T. Baikie, C. Shi, H. Ding, R. Ramesh, M. Asta, M. Graetzel, S. G. Mhaisalkar, N. Mathews, *Adv. Mater.* **2014**, 26, 7122.